



Synthesis of observed air–sea CO₂ exchange fluxes in the river-dominated East China Sea and improved estimates of annual and seasonal net mean fluxes

C.-M. Tseng¹, P.-Y. Shen¹, and K.-K. Liu²

¹Institute of Oceanography, National Taiwan University, Taipei 106, Taiwan

²Institute of Hydrological & Oceanic Sciences, National Central University, Jungli, Taoyuan 320, Taiwan

Correspondence to: C.-M. Tseng (cmtseng99@ntu.edu.tw)

Received: 3 July 2013 – Published in Biogeosciences Discuss.: 26 August 2013

Revised: 20 February 2014 – Accepted: 8 June 2014 – Published: 24 July 2014

Abstract. Limited observations exist for a reliable assessment of annual CO₂ uptake that takes into consideration the strong seasonal variation in the river-dominated East China Sea (ECS). Here we explore seasonally representative CO₂ uptakes by the whole East China Sea derived from observations over a 14-year period. We firstly identified the biological sequestration of CO₂ taking place in the highly productive, nutrient-enriched Changjiang River plume, dictated by the Changjiang River discharge in warm seasons. We have therefore established an empirical algorithm as a function of sea surface temperature (SST) and Changjiang River discharge (CRD) for predicting sea surface *p*CO₂. Syntheses based on both observations and models show that the annually averaged CO₂ uptake from atmosphere during the period 1998–2011 was constrained to about $1.8 \pm 0.5 \text{ mol C m}^{-2} \text{ yr}^{-1}$. This assessment of annual CO₂ uptake is more reliable and representative, compared to previous estimates, in terms of temporal and spatial coverage. Additionally, the CO₂ time series, exhibiting distinct seasonal pattern, gives mean fluxes of -3.7 ± 0.5 , -1.1 ± 1.3 , -0.3 ± 0.8 and $-2.5 \pm 0.7 \text{ mol C m}^{-2} \text{ yr}^{-1}$ in spring, summer, fall and winter, respectively, and also reveals apparent interannual variations. The flux seasonality shows a strong sink in spring and a weak source in late summer–mid-fall. The weak sink status during warm periods in summer–fall is fairly sensitive to changes of *p*CO₂ and may easily shift from a sink to a source altered by environmental changes under climate change and anthropogenic forcing.

1 Introduction

Continental shelves generally receive large loads of carbon from land, on the one hand, and sustain rapid biological growth and biogeochemical cycling with rates much higher than those in the open ocean, on the other hand (Walsh, 1991). Despite their relatively small total surface area ($\sim 8\%$ of the whole ocean area), they overall play a significant role in the global biogeochemical cycle as a net sink of atmospheric CO₂ ($0.2\text{--}0.5 \text{ Gt C yr}^{-1}$), which represents 10–30% of the current estimate of global oceanic CO₂ uptake (Borges et al., 2005; Cai et al., 2006; Chen and Borges, 2009; Laruelle et al., 2010). In addition, the coastal sea waters interact and exchange strongly, in complex ways, with the atmosphere and the open ocean. Thus, the environment complexities and diversity of the shelf seas pose a challenge to characterization of the dynamic carbon cycling in these regions. Based on literature compilations and global extrapolation in estimates of CO₂ sequestration in marginal seas, the aforementioned estimates existed with large uncertainties. That is because many regions are grossly undersampled, especially the mid-latitude continental shelves (Borge et al., 2010).

It was reported that continental shelves at mid- and high latitudes generally act as a sink for atmospheric CO₂, while as a source of CO₂ at low latitudes, between 30° S and 30° N. The East China Sea (ECS) is situated between the low- and mid-latitudes (between 25° N and 34° N) with an estimated overall CO₂ sink strength of $1\text{--}3 \text{ mol C m}^{-2} \text{ yr}^{-1}$ (Peng et al., 1999; Tsunogai et al., 1999; Wang et al., 2000; Shim et al., 2007; Zhai and Dai, 2009; Tseng et al., 2011). As a whole, the ECS ($\sim 0.2\%$ of global ocean area) could yield an annual

carbon uptake of 0.01–0.03 Gt C, representing 0.5–2.0 % of the global uptake. This implies a relatively high CO₂ uptake rate compared to other ocean regions. Previously reported air–sea CO₂ fluxes were, however, biased by inadequate spatial and/or temporal coverage. For instance, Tsunogai et al. (1999) first showed estimates of $\sim 3 \text{ mol C m}^{-2} \text{ yr}^{-1}$ uptake of the ECS from atmospheric CO₂ based on extrapolating from a single transect data of the PN (Pollution Nagasaki) line across the central ECS. Other later CO₂ flux studies in the ECS with uptake rates of $1\text{--}3 \text{ mol C m}^{-2} \text{ yr}^{-1}$ had been spatially limited as well (Fig. 1a). Moreover, a reliable quantification in seasonally representative CO₂ uptakes by the whole ECS has not been established to date.

The observational requirements to adequately investigate air–sea CO₂ exchange for the ECS are challenging due to the high spatial and temporal heterogeneity and complexity of the physical and biogeochemical processes (Liu et al., 2003, 2010). Sea surface $p\text{CO}_2$ ($p\text{CO}_{2w}$) distribution in the ECS is spatially/temporally variable as a result of interactions between the seasonal thermal cycle, net community production, surface/subsurface sea waters and river waters. The dominant processes in the ECS take place with typically active biological uptake of CO₂ in warm periods in the Changjiang plume area. Although higher SST favors CO₂ release to the atmosphere, better stratification favors phytoplankton growth, which draws down $p\text{CO}_2$. However, while intense physical mixing occurs in the cold season, the lower temperature increases the solubility of CO₂ in the cold seasons that overcompensates for the mixing up of CO₂ laden subsurface water, usually resulting in a net air-to-sea CO₂ flux (Tseng et al., 2011; Chou et al., 2011). In addition, $p\text{CO}_{2w}$ distribution is subjected to modification by mixing between different water masses, such as the nutrient-rich and less saline Changjiang Diluted Water (CDW, waters within 31 ‰ isohaline) and the warm, saline and nutrient-depleted waters, including the Kuroshio (KW), the Shelf Mixed (SMW) and the Taiwan Warm Current (TWC) waters (Fig. 1b). Consequently, the mixing of water masses with different biogeochemical characteristics in the ECS causes the spatial/temporal CO₂ variations (e.g., Tseng et al., 2011). Further, various circulation regimes lead to the shelf-edge processes for material exchange between the East China Sea shelf and the shelf-break hugging Kuroshio (e.g., Liu et al., 2010). Thus, to enable better quantification of the ECS CO₂ uptake capacity reiterates the need of greater spatial and temporal resolutions in observational data, which are needed for accurate estimation of air–sea CO₂ fluxes in the ECS over an annual cycle.

This study presents new data and expands on the approach of Tseng et al. (2011) of adopting innovative methods to extend the spatial and temporal coverage for broad-scale assessments of distribution and air–sea exchange fluxes of CO₂. A regional synthesis based on satellite remote sensing data (e.g., sea surface temperature, SST) calibrated with direct near-surface underway $p\text{CO}_2$ measurements and modified by the Changjiang (a.k.a Yangtze) River discharge

(CRD) has therefore been established. The CRD, as the dominant riverine nutrient source of the ECS, played a key influence on modulating the CO₂ uptake (Tseng et al., 2011). We found firstly an empirical relationship for predicting water $p\text{CO}_2$ as a function of CRD and SST. The relation was then applied to the whole ECS shelf (25–33.5° N, 122–129° E) after the model generated $p\text{CO}_{2w}$ results had been well validated against the observed $p\text{CO}_{2w}$. The resultant algorithm aimed to improve the quantification of shelf CO₂ uptake capacity in the ECS eventually leads to a time series of the air–sea CO₂ exchange flux from 1998 to 2011 that yields an annual mean value of unsurpassed accuracy after an examination of different gas-transfer algorithms.

2 Materials and methods

2.1 Analytical methods and data analyses

Thirteen seasonal cruises for direct underway atmospheric ($p\text{CO}_{2a}$) and water $p\text{CO}_2$ ($p\text{CO}_{2w}$) with hydrographic measurements were carried out in the ECS shelf (25–32° N, 120–128° E) between June 2003 and November 2011 on board R/V *Ocean Researcher I*. There was also one earlier cruise in July 1998 performing similar measurements. Most cruises ($n = 10$) were conducted in warm seasons, whereas there were also cruises conducted in each of the other seasons (spring, fall and winter). Additional data were obtained to provide the complete seasonal coverage of CO₂ distribution in the ECS. Although one-fourth of the cruises are during cold seasons, the limited cold-season data are accurate and coherent, and, therefore, representative. Essentially the cold season condition is controlled by cooling and vertical mixing, while the plume area is small. Therefore, the winter conditions are less variable in comparison to the warm season condition. In summer, by contrast, the conditions are mainly controlled by the Changjiang discharge, which is quite variable. Because the magnitude of the Changjiang plume in warm seasons determines the CO₂ uptake amount in the ECS shelf (Tseng et al., 2011), it is necessary to conduct more cruises in summer to observe the conditions with high discharges of Changjiang. Consequently, the rich summer data allow us to delineate the effect of runoff variation on the biological uptake of CO₂.

The cruise tracks and hydrographic stations superimposed on main surface currents in this study area are shown in Fig. 1b. The underway system with continuous flow equilibration, provided by the National Oceanic and Atmospheric Administration (NOAA) of the United States, is fully automated and uses gas standards (the $x\text{CO}_2$ of the four standards was 266.56, 301.76, 406.72, and 451.37 ppm, parts per million, respectively) from NOAA (Wanninkhof and Thoning, 1993). Water samples were drawn underway from the depth of about 5 m below the sea surface. The water depths of the sampling stations were greater than 30 m during all cruises.

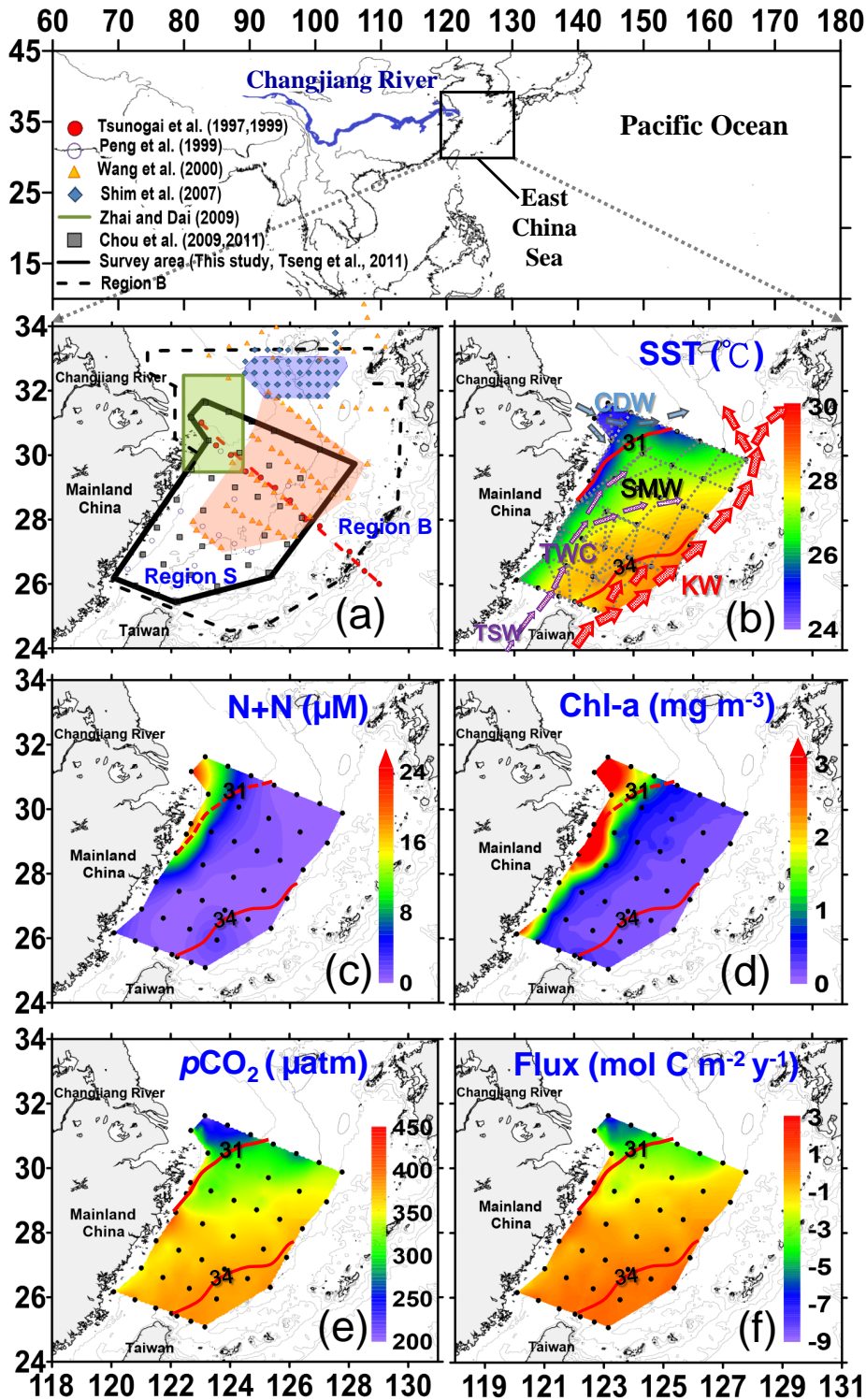


Figure 1. Maps of the study areas in the ECS showing (a) the previously published CO₂-related studies (e.g., Tsunogai et al., 1997, 1999; Peng et al., 1999; Wang et al., 2000; Shim et al., 2007; Zhai and Dai, 2009; Chou et al., 2009, 2011; Tseng et al., 2011). The surveyed area of Tseng et al. (2011) and this study is Region S. The area outlined by dashed line for modeled synthesis is Region B. (b) Hydrographic stations (black dots) and cruise track of the underway pCO₂ measurements (dashed line) with SSS and SST contours and circulation patterns in the ECS in summer. KW – Kuroshio Water; TSW – Taiwan Strait Water; TWC – Taiwan Warm Current, SMW – Shelf Mixed Water; CDW – Changjiang Diluted Water. (c) The composite distributions of surface water nutrient (N + N); (d) chlorophyll *a* (Chl *a*); (e) pCO₂; and (f) air–sea CO₂ exchange flux observed between August 2003 and July 2011 aboard R/V *Ocean Research-1* (OR1).

The precision and accuracy achieved with this method are ± 0.1 and ± 1 μatm , respectively. The distributions of sea surface salinity (SSS) and temperature (SST) were recorded using a SBE21 SEACAT thermosalinograph system (Sea-Bird Electronics Inc.). Surface chlorophyll *a* (Chl *a*) concentration was measured with a Sea Tech fluorometer attached to the Sea-Bird CTD (conductivity-temperature-depth) for a continuous in vivo fluorescence, with data calibrated by in vitro fluorometry (Turner Design 10-AU-005). Nutrient (e.g., nitrate + nitrite) and Chl *a* concentrations were measured according to Gong et al. (1996) and Tseng et al. (2005).

The time-series records including remotely sensed SST data, archived hydrographic salinity (Japan Oceanographic Data Center, JODC), wind speed (at PenGaYi Islet; 25.62° N, 122.07° E), CRD (Datong hydrological gauge station; 30.76° N, 117.62° E) and air $p\text{CO}_2$ data (Jeju Island, South Korea; 33.28° N, 126.15° E) for estimating $p\text{CO}_{2w}$ with related air–sea exchange flux in the ECS region (25–33.5° N, 122–129° E) were briefly described as below. The weekly average SST data were derived from the Advanced Very-High Resolution Radiometer (AVHRR) images from NOAA with 1 km \times 1 km resolution (<http://www.osdpd.noaa.gov/ml/ocean/sst.html>). The AVHRR SST agreed well with shipboard observations (Tseng et al., 2007, 2009a, b). The archived hydrographic salinity data in the ECS were provided by the JODC with data resolution of 1° \times 1° grids (<http://jdoss1.jodc.go.jp/cgi-bin/1997/bss>). The monthly wind speed data were estimated from the daily average data at the land-based weather station of Pen-GaYi Islet (25.62° N, 122.07° E) in the ECS provided by the Taiwan Central Weather Bureau (TCWB). The monthly CRD data at Datong hydrological gauge station (30.76° N, 117.62° E) in the lower reach of Changjiang were obtained from the Hydrological information Centre of China (<http://sqqx.hydroinfo.gov.cn/websq/>). The air $p\text{CO}_2$ was estimated from the monthly atmospheric $x\text{CO}_2$ (mole fraction) measured at Jeju Island (South Korea; 33.28° N, 126.15° E), after correction for water vapor pressure at 100% humidity with SST and salinity data (<http://www.esrl.noaa.gov/gmd/ccgg/globalview/>).

2.2 Air–sea CO₂ exchange flux estimates

Air–sea exchange flux, F , of $p\text{CO}_2$ is estimated using the equation $F = K \times \delta p\text{CO}_2$, where K (gas transfer coefficient) = kL (k : transfer velocity; L : gas solubility), $\delta p\text{CO}_2$ is the difference between the $p\text{CO}_2$ of surface water and air (i.e., $p\text{CO}_{2w} - p\text{CO}_{2a}$). The $p\text{CO}_{2a}$ was estimated from the monthly average $p\text{CO}_2$ observed at Jeju Island during the study period. Solubility of CO₂ as a function of water temperature and salinity can be estimated from the Weiss (1974) empirical equation. To obtain a more representative flux, gas transfer velocity (k) is derived using the Wanninkhof (1992, short-term formula) empirical relationship: $k = 0.31 \times u^2 \times (Sc/660)^{-0.5}$, where the Schmidt number

(Sc) is temperature-dependant for CO₂ in seawater, computed from in situ temperature data and u is the wind speed at 10 m height obtained from PenGaYi station (monthly average wind data from the TCWB database of 1998–2011). The parameterization of Wanninkhof (1992), representing a reasonable estimate for calculating wind-induced k , was firstly used for comparison with previous flux estimates in the ECS. Then, the air–sea exchange fluxes of CO₂ in the ECS reported in the previous studies were re-calculated according to the consistent wind speed data and Wanninkhof's algorithm used in this study. Finally, uncertainties of CO₂ fluxes due to using different gas-transfer algorithms (e.g., Liss and Merlivat, 1986; Wanninkhof, 1992; Wanninkhof and McGillis, 1999; Jacobs et al., 1999; Nightingale et al., 2000; McGillis et al., 2004; Ho et al., 2006; Wanninkhof et al., 2009) and their appropriate flux ranges in the ECS shelf were quantitatively evaluated.

2.3 Areal mean of $p\text{CO}_2$ and environmental variables

To obtain a representative mean value for the ECS shelf, we prepared the interpolated data set of 0.01° \times 0.01° (about 1 km \times 1 km grid points from observed $p\text{CO}_2$ and other environmental variables (e.g., SST, SSS, N + N, Chl *a* etc.) by kriging and then calculated the areal means by integrating over the survey area. The grid resolution matches the spatial resolution of weekly AVHRR-SST data. For the areal mean of the air–sea flux, we first calculated the flux within a given grid box along the cruise track for underway $p\text{CO}_2$ measurements using the average values of SST, salinity, and $\delta p\text{CO}_2$ in the box and the monthly averaged wind speed; then, we calculated the areal mean CO₂ flux over the study area in the same fashion mentioned above. Likewise, we computed the monthly flux estimates for the model study regions, encompassing almost the entire ECS (i.e., Region B: 25–33.5° N, 122–129° E, Fig. 1a), from the modeled average $p\text{CO}_2$ which was generated on a monthly basis from the CRD and SST.

3 Results and discussion

3.1 Representativeness of the study region

The ECS is a large marginal sea (25–33.5° N, 120–129.5° E) in the northwestern Pacific with an area of $\sim 0.6 \times 10^6$ km², of which three-fourths is a wide continental shelf (Fig. 1a). Our cruise region is situated in the southern and western ECS, covering an area about a half of the whole ECS. In order to evaluate whether the cruise data are representative of the entire ECS, we compared the areal mean values of AVHRR-SST from the two model areas against the observed average SST data. The two areas are respectively a small one (Region S; 25–31.5° N, 123–126° E), which is similar to the cruise survey area, and a bigger one (Region B; 25–33.5° N, 122–129° E), which covers almost the whole ECS (Fig. 1a). Briefly, the areal mean SST calculated from

observed values in cruise survey area correlated well with the average AVHRR-SST data in two model domains with perfect regression relationships ($R^2 \geq 0.98$) as shown respectively in Fig. 2a and b. It indicates, on the one hand, the remotely sensed SST data used here are reliable and validated in terms of data assurance. After calibration, the satellite SST data have overall averaged RMSEs (root mean square errors) of less than 0.5 °C (e.g., 0.37 and 0.49 °C in Regions S and B, respectively) (Fig. 2c). In the East China Sea, the differences in SST between adjacent months are, on average, about 2.3°, which is much greater than the possible errors in satellite SST. It demonstrates that errors in the remotely sensed SST do not affect significantly the calculation of the monthly variability in CO₂ solubility. On the other hand, the areal mean SST data obtained on our cruise investigations can represent the variability of the areal mean value of the entire ECS. Therefore, it is reasonable to assume that the relationship between the areal means of $p\text{CO}_2$ and mean values of hydrographic variables obtained on our cruises was also representative for the entire ECS.

The average SSS is also representative. In the river-influenced ECS shelf, most variables are strongly controlled by mixing, i.e., well correlated with SSS (Fig. 3; Tseng et al., 2011). The relationships were mostly a reflection of mixing between the Changjiang runoff and the open shelf waters (e.g., Kuroshio or TWC waters). A very good correlation between the average salinity and CRD was obtained. It is noted that a good correlation was also found between the average SSS and the area of the CDW (defined as $S < 31$). So, we can see the salinity as a proxy of CDW or vice versa. Drawdown of CO₂ occurs in the mixing zone in the open shelf, where the biological pump kicks in. The concurrent mixing and biological processes are responsible for the observed correlations. The areal mean SSS in Regions S and B are rather similar and both are representative. Briefly, the Changjiang River plume is the most important feature in the CO₂ uptake processes in the warm season, and has been well observed on our cruises, i.e., most of it has been captured in observations. As a first approximation, the peripheral regions to the north and south of the plume are more or less symmetric and, therefore, the southern shelf is representative of the whole ECS shelf. Further, we may use the aforementioned relationship to derive representative average values of $p\text{CO}_2$ for Region B, which should be the most representative for the ECS shelf.

3.2 Summer CO₂ uptake determined by Changjiang river discharge

Figure 1e and f show the composite distributions of $p\text{CO}_{2w}$ and air–sea CO₂ exchange flux from nine cruises in summer between 2003 and 2011 (see Fig. S1 for the underway measured $p\text{CO}_2$ along with cruise track). As reported previously and shown in Fig. 1, the $p\text{CO}_{2w}$ distribution in the ECS was associated with variations of water masses (Tseng et al., 2011). Lower $p\text{CO}_{2w}$ values were observed in the CDW

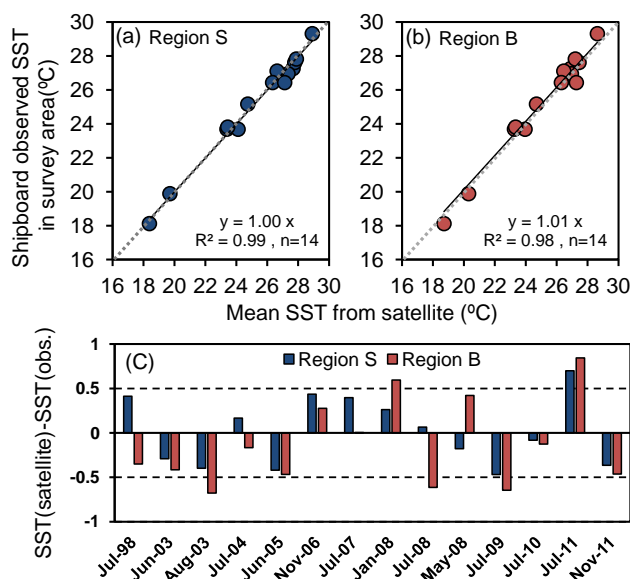


Figure 2. Linear regression relationships between areal mean AVHRR SST in two model regions, i.e., (a) S and (b) B; and field observed areal mean SST in cruise survey area (dashed line is 1 : 1 reference line). (c) Differences between the calibrated satellite data and shipboard-observed SST from 1998 to 2011.

plume area near the Changjiang River mouth and higher values in the southeastern shelf area, where saline and nutrient-depleted Kuroshio, Shelf Mixed Water and Taiwan Warm Current water prevailed. Also, the distribution of CO₂ flux in the ECS resembled that of $p\text{CO}_2$. More negative values (i.e., uptake of atmospheric CO₂ by surface water) were mostly found in the nutrient-rich river plume area with a gradual increase to the east and south. Despite the high sea surface temperature in summer that favored release of CO₂ to the atmosphere, the Changjiang River plume acted as a strong CO₂ sink, mainly due to CO₂ drawdown in the outflow region where riverine nutrients induced strong phytoplankton growth, resulting in high Chl *a* and reduced $p\text{CO}_2$ in the surface layer (Tseng et al., 2011).

The results obtained through the statistic correlation analyses (Table 1) and figures (Figs. 3, 4) for areal means of $p\text{CO}_2$ and other environmental variables further demonstrate that the biological sequestration of CO₂ in the warm periods, as indicated by the relatively low summer $p\text{CO}_2$, was well correlated to the CRD. Figure 4 also illustrates that the whole ECS CO₂ uptake was significantly correlated with the CDW area, the Changjiang discharge, the amounts of N + N or the mean Chl *a* in summer. The relationship between CO₂ uptake and nutrients suggest that the observed nutrient concentration supported the DIC (dissolved inorganic carbon) uptake, even when the surface was warming and favored CO₂ outgassing. Eventually, the biological effect outweighs the warming effect. Through the first-order estimation, the ratios (C/N) of the amount of nutrient discharged over the

Table 1. Correlation coefficient matrix for areal means of $p\text{CO}_2$ and other environmental variables in the ECS shelf in summer months from 1998 to 2011 ($n = 10$).

	*CRD	CDW area ($S < 31$)	Sea-to-air CO ₂ Flux	$\delta p\text{CO}_2$	$p\text{CO}_{2w}$	N + N	Chl <i>a</i>
CRD	1.00						
CDW area	0.91	1.00					
Sea-to-air CO ₂ Flux	−0.97	−0.89	1.00				
$\delta p\text{CO}_2$	−0.92	−0.83	0.94	1.00			
$p\text{CO}_{2w}$	−0.98	−0.80	0.94	0.96	1.00		
N + N	0.70	0.88	−0.71	−0.75	−0.73	1.00	
Chl <i>a</i>	0.88	0.60	−0.65	−0.81	−0.82	0.72	1.00

* Average Changjiang River discharge data collected at Datong station during the LORECS cruise period. Regression results between other variables and Changjiang discharge were obtained for the ten cruises, not including OR1-686 (19–26 June 2003). Before that cruise, the Typhoon Soudelor (16–18 June 2003) passed over east of the ECS shelf toward Korea and Japan. Such a typhoon effect anomalously induced the more diluted plume area through enhanced rainfall in the lower watershed of Changjiang below Datong station. However, high typhoon-induced discharge was not recorded at Datong which is 624 km upstream from the river mouth.

amount of CO₂ taken up by the sea in July or during the warm period are between 5 and 7, which agrees well with the Redfield ratio. The preliminary results show that the nutrient fluxes (July: nitrate, 9.9 Gmol under averaged CRD 45 000 m³ s^{−1}; warm periods: 51 Gmol under 39 000 m³ s^{−1}) discharged to the sea were enough to support the DIC uptake estimated by air–sea exchange (July: 44 Gmol under the uptake rate of 0.88 mol C m² yr^{−1}; warm period: 360 Gmol under 1.21 mol C m² yr^{−1}). Please note that near-shore areas in the low salinity zone of the Changjiang plume with strong respiration (Zhai et al., 2009) and the coastal upwelling zone (Chou et al., 2009) had high $p\text{CO}_2$ values. However, the outgassing areas (< 4 % of the ECS shelf area) were very small relative to the CO₂ uptake areas in the open shelf based on the weighted statistic analyses. It barely changes the net sink terms at all. Consequently, the CO₂ distribution/uptake dynamics were associated yearly with the changes of the plume expansion determined by the CRD:

$$p\text{CO}_2 = -3.9 \times \text{CRD} + 517, \quad R^2 = 0.97, \quad n = 9; \quad (1)$$

$$\text{CO}_2 \text{ flux} = -0.19 \times \text{CRD} + 7, \quad R^2 = 0.95, \quad n = 9. \quad (2)$$

where CRD is in units of 10³ m³ s^{−1}. The results demonstrate again that Changjiang River discharge governs coastal ocean production and CO₂ uptake capacity in the East China Sea shelf in summer.

3.3 Empirical algorithm to simulate seasonal $p\text{CO}_{2w}$ variations

To derive representative mean values of $p\text{CO}_{2w}$ in different seasons in the entire ECS shelf, we may use the strong correlation between river discharge and CO₂ uptake mentioned above (e.g., Tseng et al., 2011). We thus developed an empirical algorithm by using the monthly areal mean (referred

to as “average” hereafter) of observed $p\text{CO}_{2w}$, SST and the CRD during warm periods. The data mentioned above were collected during warm cruises between May and November between 1998 and 2011. Firstly, we found normalized $p\text{CO}_2$ at 25 °C ($Np\text{CO}_2$) correlated negatively with the CRD ($\times 10^3 \text{ m}^3 \text{ s}^{-1}$) with a good regression relationship (Fig. 5) as follows:

$$Np\text{CO}_2 \text{ at } 25^\circ\text{C} = -2.71 \times \text{CRD} + 427 \quad (R^2 = 0.93). \quad (3)$$

Here, $Np\text{CO}_2$ at 25 °C, which is the observed average $p\text{CO}_{2w}$ normalized to a constant temperature of 25 °C (mean SST of all cruises), was computed by using the following equation proposed by Takahashi et al. (1993):

$$Np\text{CO}_2 \text{ at } T_{\text{mean}} = (p\text{CO}_{2w})_{\text{obs}} \times \exp[0.0423(T_{\text{mean}} - T_{\text{obs}})], \quad (4)$$

where T_{mean} is 25 °C and T_{obs} is the observed monthly mean value and $(p\text{CO}_{2w})_{\text{obs}}$ is the observed average $p\text{CO}_{2w}$. The purpose of “ $p\text{CO}_2$ normalized to 25 °C” is to eliminate the temperature effect in order to discern other factors (e.g., biological activities, air–sea exchange and vertical transport of subsurface waters etc.) that affect $p\text{CO}_2$.

The inversely linear relationship between the $Np\text{CO}_2$ and CRD during warm periods as shown by Eq. (1) indicates that $p\text{CO}_{2w}$ changes in the ECS shelf water were mainly governed by biological processes, while other processes, such as the upward transport of DIC from subsurface waters and the air–sea CO₂ exchange, are minimal under strong stratification.

We finally refined the empirical algorithm for predicting $p\text{CO}_{2w}$ according to Eqs. (3) and (4) as below,

$$p\text{CO}_{2w} = (-2.71 \times \text{CRD} + 427) \times e^{[0.0423 \times (T_{\text{obs}} - 25)]}, \quad (5)$$

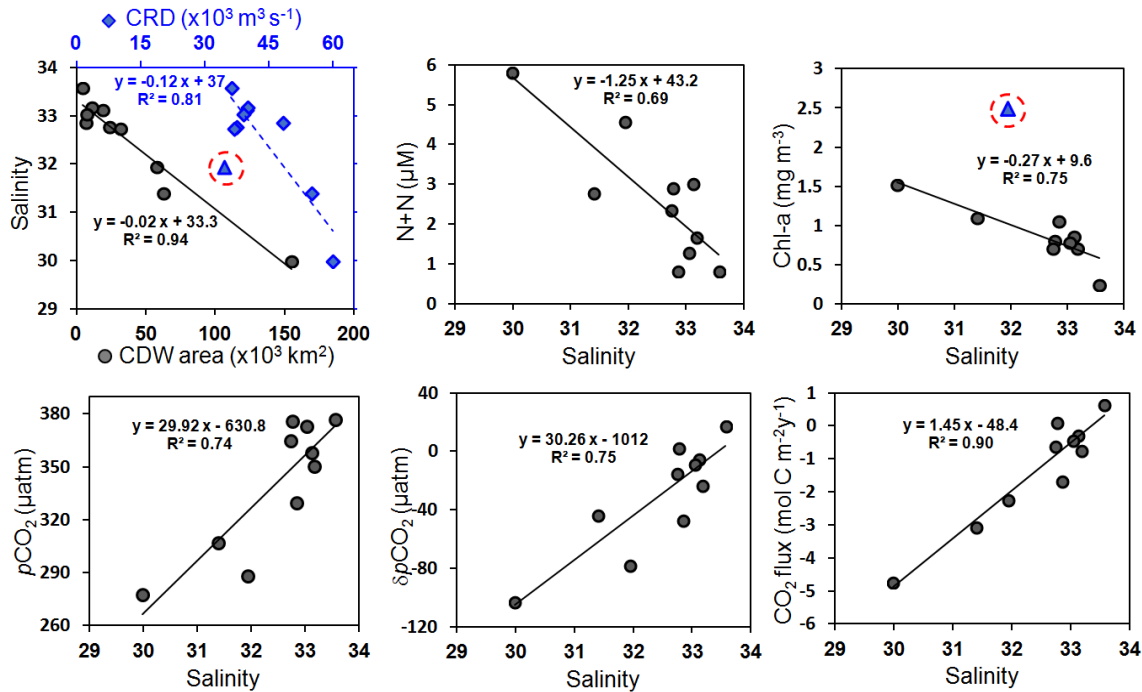


Figure 3. Relationships between areal mean SSS and hydrographic variables in the whole ECS. (*A triangle denotes the data obtained from the cruise of OR1-686 (19–26 June 2003). In the plot of Chl *a* vs. salinity, the circled triangle is an outlier that was not included in the regression analysis. The outlier was probably caused by the Typhoon Soudelor (16–18 June 2003) that passed over the eastern ECS shelf right before the cruise. The anomalously low salinity was probably caused by the typhoon rain instead of the river discharge, while the high Chl *a* level was probably caused by typhoon-driven vertical mixing rather than river discharged nutrients.

where -2.71 is the slope obtained from the plot of $NpCO_2$ versus CRD; CRD is the Changjiang River discharge in units of $10^3 \text{ m}^3 \text{ s}^{-1}$; T_{obs} is the monthly average AVHRR SST. As mentioned above, the pCO_2 estimates should be reasonable since the bias in AVHRR SST has been minimized (lower than 0.5°C ; an estimated error of $< 10 \mu\text{atm}$; Fig. 2c).

However, when we applied the same relationship to the cold season, we found that the relationship underestimated the $NpCO_2$ (Fig. 3). The extra increment was probably mainly caused by the increase in DIC provided by enhanced vertical mixing in the cold season. It is necessary to compensate for the mixing effect in the equation. As shown in Fig. 3, an increase of $57.4 \mu\text{atm}$ was needed to reach the observed $NpCO_2$ of $455.1 \mu\text{atm}$ for January from the computed $NpCO_2$ of $397.7 \mu\text{atm}$, which was calculated from the CRD of $10211 \text{ m}^3 \text{ s}^{-1}$. This increment represents a 14.4% increase to account for the mixing replenishment.

For the model calculation, the seasonal mixing contribution could be estimated from the data of wind speed (W) and remotely sensed SST (T) through the relationship between the mixing ratio and the mixing index defined as W/T (Fig. 6). We firstly found a significant correlation between climatological monthly averaged mixed layer depth (MLD) data obtained from the Ifremer/Los Mixed Layer Depth Climatology website (http://www.ifremer.fr/cerweb/deboyer/mld/Surface_Mixed_Layer_Depth.php) and

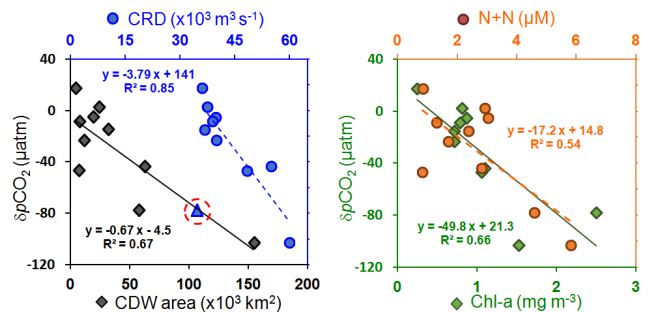


Figure 4. Relationships between δpCO_2 and (a) the CDW plume area or the CRD; and (b) $N+N$ and Chl *a* in summer from July 1998 to July 2011 in the ECS shelf. “—” indicates uptake of CO_2 by shelf water from the atmosphere. The best-fit lines by a linear regression analysis ($n = 10$, all p values < 0.001) are shown in the plume area and Chl *a* (solid line) and in CRD and $N+N$ (dashed line), respectively. The CRD denotes average Changjiang River discharge data collected at Datong station during the LORECS cruise period. The blue circled triangle denotes the data point from the OR1-686 cruise, which was excluded from the regression analysis.

the mixing index; and then those collected from field observations were well-fitted in the regression range as well (Fig. 6a). It indicates the surface MLD, where turbulence is generated by winds and surface heat fluxes, positively

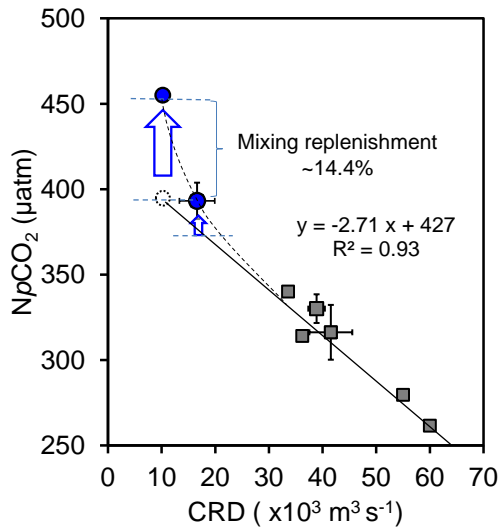


Figure 5. The correlation between monthly average $NpCO_2$ and CRD (black square) was observed during warm cruises from May to November between 1998 and 2011: observed $NpCO_2$ about 455.1 μatm (blue dot) and the computed $NpCO_2$ 397.7 μatm (dotted circle) at the CRD at $10211 \text{ m}^3 \text{ s}^{-1}$ during the January cruise.

correlates to W and negatively to T , i.e., $\text{MLD} \propto W/T$ as the mixing index. Further, the computed MLDs estimated by the $\text{MLD}-W/T$ relationship are in excellent agreement with observations and climatologic averages (Fig. 6b). It indicates the mixing index as wind versus SST (W/T) shall be considered as a proper vertical mixing parameter. The seasonal mixing ratio as a function of mixing index further follows an arctan curve made by the inverse tangent function: mixing ratio (%) = $(\tan^{-1}[61.2(W/T) - 23] + 1.5)/20$ (Fig. 6c). Overall, the greatest contribution of the mixing replenishment is ca. 14.4% due to strongly vertical mixing in cold months (e.g., January, February and March) in the ECS shelf, when the SST is the lowest and wind speed highest during the northeast monsoon (Fig. 6d). During warm periods, the contribution of the mixing tends to almost zero due to a strong stratification. A distinctly seasonal change in mixing contribution will occur during the monsoon transition/season, alternating from the cold to the warm periods or vice versa.

3.4 Time series of model results vs. field observations

Tseng et al. (2011) demonstrated the Changjiang plume size is directly governed by the Changjiang River discharge (Table 1; Fig. 3a). Intraseasonal variations in plume area were hence observed due to intraseasonal changes in the Changjiang River discharge. Additionally, both water pCO_2 and $NpCO_2$ during the warm period were all well correlated with Changjiang River discharge (Figs. 3, 4). The discharge, which governs the nutrient inputs into the ECS, is the primary factor to control the CO₂ uptake of the whole ECS. In summary, the focus on $NpCO_2$ during the productive pe-

riod in summer is bound to emphasize the river's effect (i.e., high river discharge, causing high nutrient inputs and inducing phytoplankton growth) on biological export. Therefore, although we conducted only one cruise between 1998 and 2002, the general feature of the river effect on the CO₂ uptake in the river-dominated ECS system should be applicable.

The 14-year time series of model results of monthly mean pCO_{2w} , δpCO_2 and the air–sea CO₂ flux in Regions S and B over the study period (1998–2011) are shown in Fig. 7, in which mean observed values of the 14 cruises are also plotted for comparison. It is clear that all modeled pCO_{2w} , δpCO_2 and the CO₂ flux agree well with the observations (Fig. 7; Supplement Fig. S2). The good linear relationships between the modeled areal means and the means of observed values confirm the satisfactory performance of the empirical algorithm, which has been applied to both the small and big domains (S and B) of the ECS (Supplement Fig. S2). The uncertainty resulting from parameterization of the mean pCO_2 may be indicated by the root mean square of the deviations between the model results and observations, which was found to be 13.4 μatm ($n = 14$). It is noted that the mean deviation, 0.7 μatm , was quite small.

As shown in Fig. 7b, the time series is characterized by a distinct seasonal pattern with a maximum in late summer–mid-fall and a minimum in spring. In general, the pCO_{2w} mostly remained below pCO_{2a} throughout an annual cycle except during the period from late summer to mid-fall. That means the evasion of CO₂ occurred primarily in a relatively short period in the warm season. Moreover, the amount of CO₂ released was small relative to the drawdown of CO₂ in other seasons. The δpCO_2 , which represents a driving potential for CO₂ gas transfer across the water–air interface, seasonally fluctuated with a slight supersaturation of about +10 μatm , signifying a source of CO₂ from the ECS to atmosphere, on average in late summer to mid-fall and a strong undersaturation of –80 μatm , signifying a sink of atmospheric CO₂, in spring (Fig. 7c).

There were also apparent interannual variations, which showed unusually high peak values in 2001, 2006 and 2011 (drought years) and exceptionally low values in 1998 and 2010 (flood years). There were anomalously strong supersaturations observed in the late summers of 2001, 2006 and 2011 and undersaturation in the summer of 1998 and late spring of 2010, respectively, due to the Changjiang discharge fluctuations caused by climate change (Tseng et al., 2011). Subtle long-term increasing trends in pCO_{2a} and pCO_{2w} were distinctly observed:

$$pCO_{2a} = 1.9(\pm 0.0) \times t + 353.4(\pm 0.2), \quad r^2 = 0.99, \quad n = 14; \quad (6)$$

$$pCO_{2w} = 2.1(\pm 0.8) \times t + 309.5(\pm 6.8), \quad r^2 = 0.36, \quad n = 14, \quad (7)$$

where $t = \text{year} - 1997$. The pCO_{2a} has been increasing from 355.5 to 380.7 μatm at a rate of 1.9 $\mu\text{atm yr}^{-1}$, or 5.3 $\% \text{ yr}^{-1}$, which is comparable to those observed at the Mauna Loa Observatory ($\sim 5.1 \% \text{ yr}^{-1}$) during the study period. The

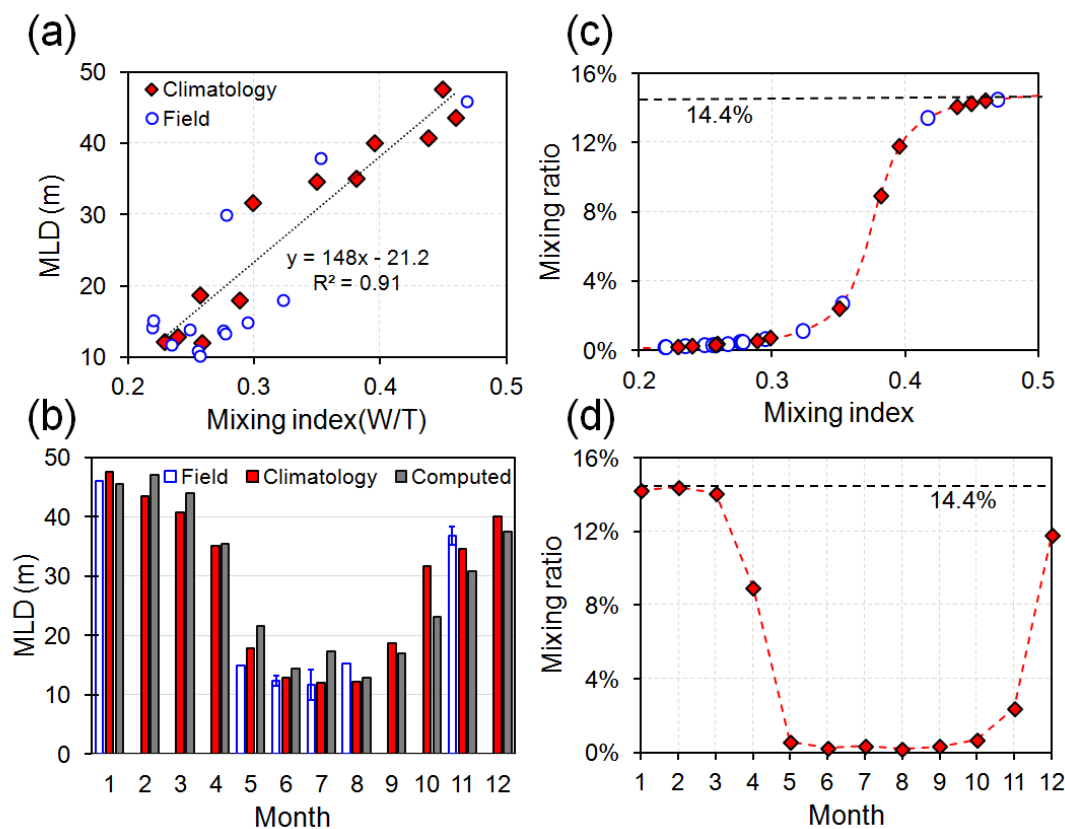


Figure 6. (a) Relationship between averaged MLD obtained from monthly climatology and field observations and mixing index (W/T). (b) Comparison of the computed MLD with those from climatology and field. (c) Arc tangent relationship between the mixing index and contribution ratio. Blue dot: field surveys; red diamond: climatology monthly averages. (d) Monthly variability in the contribution ratio of vertical mixing in the ECS.

$p\text{CO}_{2a}$ seasonality shows a spring high and a summer low. Please note the atmospheric $p\text{CO}_2$ observed from the cruise correlated well with the time-series data measured at Jeju Island (field $p\text{CO}_{2a}$ (LORECS) = $1.01 \times p\text{CO}_{2a}$ (Jeju), $R^2 = 0.90$, $n = 13$; Fig. 7b). The rate of increase in $p\text{CO}_{2w}$ of about $2.1 \mu\text{atm yr}^{-1}$ was slightly higher than that in $p\text{CO}_{2a}$ during the study period so that $\delta p\text{CO}_2$ results showed an increase at a rate of $0.2 \mu\text{atm yr}^{-1}$. The increasing $\delta p\text{CO}_2$ can in part be due to decreasing CRD under environmental changes, e.g., the operation of Three Gorges Dam and the water transferring scheme from south to north in China (Tseng et al., 2011). Eventually, if this trend is true and it continues, the uptake in the ECS will gradually decrease.

The surface $p\text{CO}_{2w}$ and $\delta p\text{CO}_2$ (summarized in Table 2) varied seasonally and interannually in the ECS shelf. The annual pattern in $\delta p\text{CO}_2$ shows that negative $\delta p\text{CO}_2$ occurs in the whole year. Overall, the ECS shelf serves as a net sink of atmospheric CO₂ with $-38 \pm 13 \mu\text{atm}$ of $\delta p\text{CO}_2$ on average, with a strong sink in winter ($-43 \pm 12 \mu\text{atm}$) and spring ($-75 \pm 12 \mu\text{atm}$), and a weak sink in summer ($-28 \pm 33 \mu\text{atm}$) and fall ($-6 \pm 15 \mu\text{atm}$). Data from a few other cruises (spring, fall and winter) will also be used to

show the complete seasonal CO₂ distribution in this region (Fig. 7c; Table 3). The average annual $\delta p\text{CO}_2$ was calculated to be about $-46 \pm 45 \mu\text{atm}$ with the seasonal variability at ca. -109 , -25 ± 39 ($n = 3$), -6 , and $-46 \mu\text{atm}$ for spring, summer, fall, and winter, which were consistent with those estimated by model. The seasonal pattern shows a sink-to-source transition in late summer–mid-fall during the Changjiang River plume reduction after the July maximum discharge (see Fig. 9; Tseng et al., 2011). Furthermore, the weak sink status during warm periods is fairly sensitive to changes of $p\text{CO}_2$ and to become a CO₂ source due to the Changjiang discharge decreases through environmental changes (Tseng et al., 2011).

3.5 Comparison with previous estimates

Figure 8 further shows the comparison of $\delta p\text{CO}_2$, in the same month of certain years between the data retrieved from published references and this study and those generated by the model. For a comparison on an equal basis, the reported fluxes had been recalculated using the consistent source of monthly wind speed data from PenGaYi station in the ECS and the Wanninkhof's gas transfer algorithm (1992,

Table 2. The seasonal and annual average CO₂ results between 1998 and 2010 in the ECS shelf.

Year		1998	1999	2000	2001	2002	2003	2004
<i>p</i> CO _{2w} (μ atm)	Spring	283 \pm 18	305 \pm 18	302 \pm 12	296 \pm 13	284 \pm 25	295 \pm 17	308 \pm 6
	Summer	265 \pm 15	281 \pm 31	340 \pm 28	381 \pm 45	314 \pm 14	335 \pm 45	358 \pm 27
	Fall	335 \pm 41	332 \pm 19	338 \pm 10	359 \pm 28	346 \pm 23	363 \pm 13	353 \pm 5
	Winter	342 \pm 15	328 \pm 24	328 \pm 25	328 \pm 17	316 \pm 17	331 \pm 9	333 \pm 34
	Annual	299 \pm 38	314 \pm 30	328 \pm 24	340 \pm 42	317 \pm 29	328 \pm 35	340 \pm 26
δp CO ₂ (μ atm)	Spring	-77 \pm 18	-58 \pm 17	-62 \pm 13	-69 \pm 12	-84 \pm 25	-75 \pm 16	-65 \pm 7
	Summer	-86 \pm 12	-72 \pm 31	-14 \pm 31	25 \pm 48	-44 \pm 18	-25 \pm 49	-4 \pm 31
	Fall	-18 \pm 36	-22 \pm 15	-17 \pm 8	3 \pm 32	-12 \pm 26	1 \pm 14	-9 \pm 7
	Winter	-19 \pm 16	-35 \pm 25	-36 \pm 27	-38 \pm 19	-52 \pm 19	-40 \pm 10	-38 \pm 36
	Annual	-57 \pm 37	-44 \pm 29	-31 \pm 27	-20 \pm 47	-46 \pm 32	-37 \pm 39	-27 \pm 31
Year		2005	2006	2007	2008	2009	2010	Average
<i>p</i> CO _{2w} (μ atm)	Spring	296 \pm 5	300 \pm 6	312 \pm 6	296 \pm 16	300 \pm 10	280 \pm 19	297 \pm 10
	Summer	344 \pm 34	368 \pm 56	347 \pm 11	359 \pm 29	346 \pm 20	298 \pm 32	334 \pm 34
	Fall	346 \pm 12	395 \pm 24	375 \pm 24	350 \pm 19	382 \pm 10	357 \pm 9	356 \pm 19
	Winter	330 \pm 15	342 \pm 20	335 \pm 18	331 \pm 9	323 \pm 8	315 \pm 6	329 \pm 8
	Annual	328 \pm 28	349 \pm 47	343 \pm 27	334 \pm 30	339 \pm 33	314 \pm 34	329 \pm 14
δp CO ₂ (μ atm)	Spring	-79 \pm 5	-77 \pm 5	-67 \pm 7	-84 \pm 16	-82 \pm 10	-105 \pm 18	-75 \pm 12
	Summer	-20 \pm 39	2 \pm 62	-19 \pm 15	-11 \pm 33	-25 \pm 25	-76 \pm 37	-28 \pm 33
	Fall	-19 \pm 12	28 \pm 29	7 \pm 19	-20 \pm 22	10 \pm 14	-17 \pm 15	-6 \pm 15
	Winter	-45 \pm 16	-35 \pm 22	-43 \pm 19	-49 \pm 10	-59 \pm 10	-67 \pm 6	-43 \pm 12
	Annual	-41 \pm 33	-22 \pm 52	-30 \pm 31	-41 \pm 35	-37 \pm 38	-65 \pm 38	-38 \pm 13

short-term formula). In addition, the Changjiang discharges in reported references were plotted in the discharge range of the climatological monthly mean with ± 1 standard deviation (SD; 1998–2010) as a reference level to check anomalous events (Fig. 9a). The results show there were three flood surveys obtained in July 1992, 1998 and 2010 and others mostly fell within ± 1 SD range of the climatological mean. As a whole, most of the published *p*CO₂ values are erratic away from 1 : 1 reference line outlier levels of $\pm 20 \mu\text{atm}$ (e.g., Peng et al., 1999; Wang et al., 2000; Shim et al., 2007; Zhai et al., 2009) while some are close to model outputs (e.g., Tsunogai et al., 1999; Wang et al., 2000, in summer; Chou et al., 2011; this study). The estimates with large uncertainties are mainly due to inadequate representativeness of the spatial variability and limited sampling resolution. These problems in each report are briefly summarized in the remarks in Table 3 and the following text.

Tsunogai and coworkers (1997, 1999), for instance, reported the air–sea exchange fluxes of CO₂ in the whole ECS were only extrapolated from a single transect data set of the PN line across the northern ECS (Fig. 1a; Table 3). Therefore, the findings in summer and winter applied to the whole ECS from one survey line certainly cause biases and slightly higher values than the model ones (Fig. 9b, c). Their developed algorithm was not suitable for the use of the near-shore waters. Likewise, the *p*CO₂ data of Peng et al. (1999) were all generated from the TA and TCO₂ which were only collected in spring and limited in low-resolution samplings.

Moreover, the study area of Peng et al. (1999) was mostly located in the Kuroshio, Mixed Shelf and Taiwan Warm Current waters and lacked coverage of coastal plume waters. Higher results in spring than those by the model were therefore found (Fig. 9b, c), since coastal plume processes which drew the CO₂ low via phytoplankton blooms near the Changjiang River mouth were not observed.

Wang et al. (2000) had only two field observations in spring and summer, while their fall and winter data were computed from Tsunogai's empirical algorithm. Their observations lacked data from the coastal waters, although they had a wide-area survey (Fig. 1a). Hence, the spring *p*CO₂ data in the whole ECS, being derived from a temperature-dependent relationship, were higher than those by the model, which could not reflect the biological uptake by plankton blooms in the Changjiang plume (Fig. 9b, c). The summer results derived from the salinity relationship were lower than the modeled ones. That was because of lack of the data from additional replenishment of CO₂ from subsurface waters by coastal upwelling. Additionally, the fall and winter data derived from Tsunogai's algorithm could not reflect the additional CO₂ by vertical mixing during the cold seasons. Therefore, those data generated from Tsunogai's algorithm were lower than our data by model and field observation (Fig. 9b, c).

The study in Zhai and Dai (2009) was focused on the areas near the Changjiang estuary so that the *p*CO₂ data had large fluctuations due to complexities of coastal processes

Table 3. Summary of the CO₂ results in the ECS reported in the previous studies and obtained from this study.

References	Study seasons	Sampling times	Field		Model		Remarks
			^a $\delta p\text{CO}_2$	^b Flux	$\delta p\text{CO}_2$	Flux	
Tsunogai et al. (1997, 1999)	Summer	Aug 1994	15	1.0	1	0.1	1. Measured CO ₂ parameters: DIC, total alkalinity (TA), $p\text{CO}_2$ 2. One single transect-PN line from 31.4° N, 123° E to 27.5° N, 128.4° E
	Winter	Feb–Mar 1993	–44	–2.4	–39	–2.2	
	Fall	Oct 1993 Nov 1995	–26 –7	–1.3 –0.4	–19 –15	–0.9 –0.8	
	Annual mean	1993–1995	–55	–2.4	–36	–1.5	
Peng et al. (1999)	Spring	May 1996	–28	–1.7	–90	–2.8	1. DIC, TA 2. Two major mutually vertical transects from north–south and east–west with 14 stations in central ECS
Wang et al. (2000)	Spring	May 1995	^c –33 ^d (–37)	–0.9 (–0.9)	–89	–2.8	1. DIC, TA 2. Wide-area survey in central and northern ECS with 26–49 stations 3. Lack of coastal and estuarine data
	Summer	Jul 1992	^c –13 ^e (–37)	–0.6 (–1.7)	–45	–2.1	
Shim et al. (2007)	Spring	May 2004	–47	–1.5	–62	–1.9	1. $p\text{CO}_2$ 2. Parts of northern ECS (32–34° N, 124–128° E)
	Summer	Aug 2003	–23	–0.9	31	1.2	
	Fall	Oct 2004	11	0.8	–3	–0.2	
		Nov 2005	4	0.2	–26	–1.4	
Zhai and Dai (2009)	Spring	Mar 2008	–38	–1.5	–76	–3.0	1. $p\text{CO}_2$ 2. Outer Changjiang estuary in the inner shelf of the northwestern ECS (30–33° N, 122–124° E)
		Apr 2005	–10	–0.4	–84	–3.1	
		Apr 2008	–79	–3.1	–103	–4.0	
		May 2005	–67	–2.4	–74	–2.5	
		Mean	–48	–1.8	–84	–3.1	
	Summer	Jul 2007	–74	–2.4	–10	–0.3	
		Aug 2003	–45	–1.7	31	1.2	
		Mean	–60	–2.1	10	0.4	
	Fall	Sep 2006	22	1.1	53	2.2	
		Oct 2006	–45	–2.7	35	1.3	
		Nov 2006	4	0.2	–3	–0.1	
		Nov 2007	64	5.7	27	–2.4	
Mean	11	1.1	28	1.4			
Winter	Jan 2006	–37	–2.3	–51	–3.1		
Chou et al. (2009, 2011)	Summer	Jul 2007	–37 ^c (–26)	–2.3 (–1.2)	–10	–0.3	1. DIC, TA, PH (summer); DIC, TA, PH, $p\text{CO}_2$ (winter) 2. The more complete ECS with 40 stations (25–32° N, 120–128° E)
	Winter	Jan 2008	–46	–3.0	–36	–2.4	
This study (Tseng et al., 2011)	Spring	May 2009	–109	–3.4	–82	–2.6	1. $p\text{CO}_2$ 2. The more complete ECS area (25–32° N, 120–128° E)
	Summer	Jun 2003	–77	–2.2	–57	–1.7	
		Aug 2003	17	0.6	31	1.2	
		Jul 2004	–5	–0.3	–2	–0.1	
		Jun 2005	–47	–1.7	–65	–2.3	
		Jul 2007	–23	–0.7	–10	–0.3	
		Jul 2008	3	0.2	10	0.5	
		Jul 2009	–8	–0.4	–18	–0.9	
		Jul 2010	–103	–4.7	–88	–3.9	
	Fall	Jul 2011	–15	–0.6	–4	–0.1	
		Nov 2006	–15	–0.6	–3	–0.1	
	Winter	Nov 2011	4	0.2	–7	–0.4	
		Jan 2008	–46	–3.0	–36	–2.4	

^a Units in $\delta p\text{CO}_2$ and CO₂ flux are μatm and $\text{mol C m}^{-2} \text{ yr}^{-1}$, respectively;

^b Recalculated by wind speed data at PenGaYi and Wanninkhof's gas transfer algorithm (1992, short-term formula);

^c Average of all stations;

^d Averaged by values derived from $p\text{CO}_2$ –salinity relationship;

^e Averaged by values derived from $p\text{CO}_2$ –SST relationship.

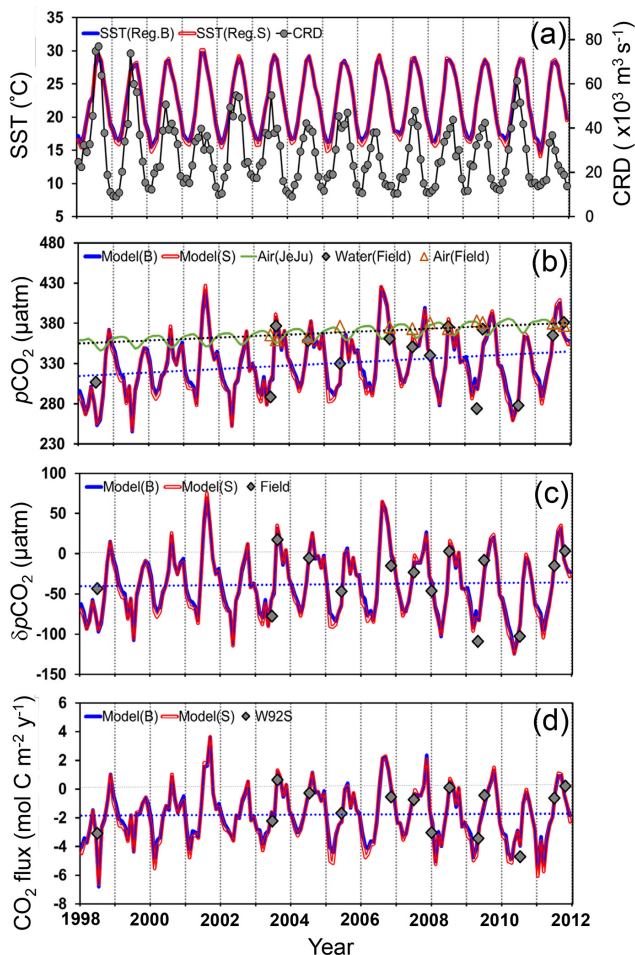


Figure 7. Time-series variations (model results with observed data of 14 cruises) in monthly areal mean (a) SST and CRD, (b) $p\text{CO}_{2w}$ and $p\text{CO}_{2a}$, (c) $\delta p\text{CO}_2$, and (d) CO_2 flux in the sea surface of the ECS shelf (“+”: sea to air; “-”: air to sea) between 1998 and 2011. The tick on the time axis corresponds to 1 January of the year marked.

with plume dynamics (Fig. 8). Low summer data were, for example, observed due to a strong bio-uptake of CO_2 relative to data for the whole ECS, while high $p\text{CO}_2$ in fall was due to a strong vertical mixing (Fig. 9b, c). The data of Shim et al. (2007) which were collected in the northeastern ECS is lower in summer and higher in spring, fall and winter than model ones (Fig. 9b, c). That might be attributed to more dispersion of the Changjiang plume to the northeast of the ECS in summer, at the period of drawdown, and the more intensive vertical mixing induced by the colder SST in cold seasons to bring the more enriched- CO_2 subsurface water to the surface, respectively. The comparison results further indicate small-scale spatial surveys which were performed in the Changjiang estuary and northern ECS area could not be representative of the whole ECS shelf.

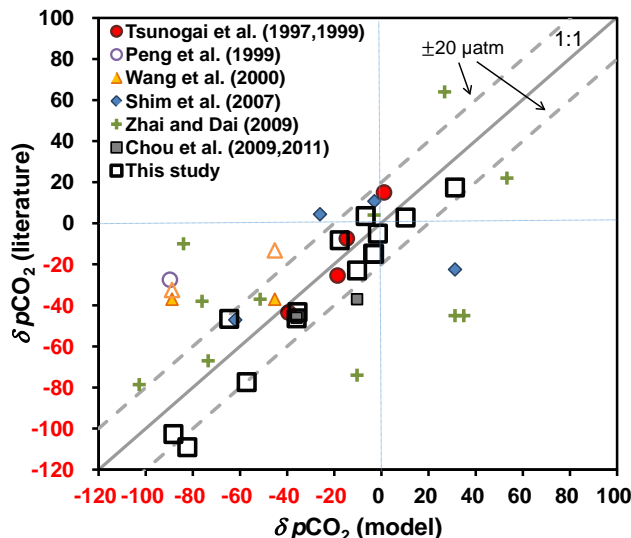


Figure 8. $\delta p\text{CO}_2$ comparison between the data retrieved from published references and this study and those generated by the model at the same surveying time.

Chou et al. (2011) covered the more extensive areas like our study area so that the areal mean fluxes were rather consistent with ours. After all, the outputs from our algorithm were validated by our field observations of in situ underway $p\text{CO}_2$ with high spatial and temporal resolutions since 2003 (Fig. 7b, c, d). The model $p\text{CO}_{2w}$ results agreed well with the observed $p\text{CO}_{2w}$ ($R^2 = 0.90$, $n = 14$; Fig. 7b). In addition, our algorithm can reflect the results caused by anomalous flood events, e.g., the floods of July in 1998 and 2010 causing exceptionally low $p\text{CO}_{2w}$ values and high CO_2 uptakes (Table 2; Fig. 9a, b, c). Therefore, this assessment of annual CO_2 uptake is more credible than all previous estimates ($1\text{--}3 \text{ mol C m}^{-2} \text{ yr}^{-1}$) since our better spatial and temporal coverage reduces uncertainties.

3.6 Comparison with flux estimates by different gas-exchange algorithms

Factors that affect air–sea CO_2 flux estimates using the two-layer gas exchange model are mainly from two parts: (1) environmental forcing factors that control the gas transfer velocity, k (m s^{-1}), and (2) thermodynamic driving potentials that affect air–sea $p\text{CO}_2$ concentration differences (Wanninkhof et al., 2009). Among these, the parameterizations for k as a function of wind speed are largely empirical with inherent sources of uncertainty and therefore have a critical effect on the reliability of the flux estimates. Different relationships of gas exchange with wind were empirically developed by the different approaches to calculate the gas-transfer velocity over the past decades (e.g., Liss and Merlivat, 1986 (hereafter LM86); Wanninkhof, 1992 (W92: W92S, short-term; W92L, long-term); Wanninkhof

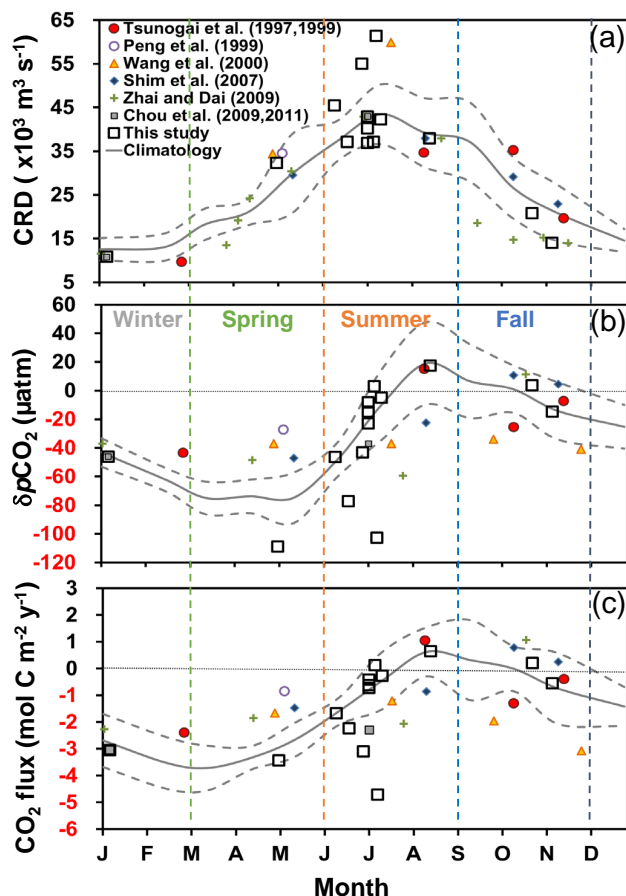


Figure 9. Seasonal monthly patterns revealed in observational data of (a) CRD, (b) $\delta p\text{CO}_2$ and (c) air–sea CO_2 flux, obtained from published references and from field data in this study and model results. The thick curves denote the climatological mean and the dashed curves denote the range of ± 1 SD during the study period of 1998–2011.

and McGillis, 1999 (WM99: WM99S; WM99L); Jacobs et al., 1999 (J99); Nightingale et al., 2000 (N00); McGillis et al., 2004 (M04); Ho et al., 2006 (H06); Wanninkhof et al., 2009 (W09)). The plot of different algorithms for k against wind speed, as shown in Fig. 10, reveals that the differences among the algorithms significantly increase with increasing wind speed, i.e., at low wind speeds they are much less than those at high wind speeds ($> 10 \text{ m s}^{-1}$). In this study, the monthly average wind speed obtained from PenGaYi station in the ECS ranged between 5 and 11 m s^{-1} with stronger winds in cold seasons during the northeast monsoon (Fig. 10). Varying up to almost threefold of differences among different algorithms for the calculation, the wind-induced k was calculated to be the highest by J99 and lowest by LM86. It further demonstrates the largest source of uncertainties involved in estimating air–sea CO_2 flux resides with these algorithms. Particularly, the differences would increase drastically among the models developed by J99, W92L and

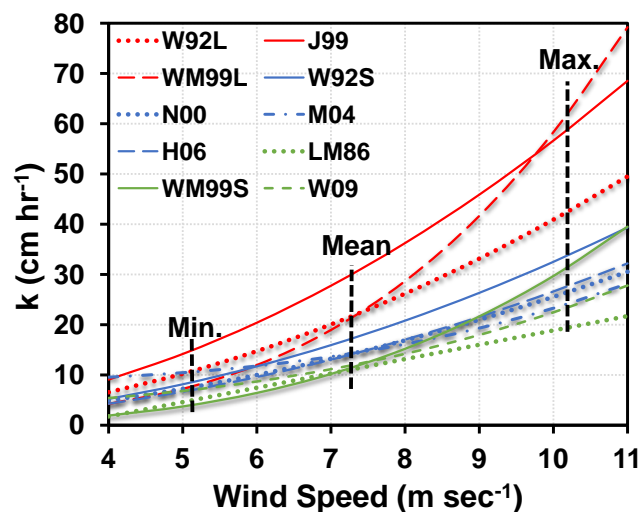


Figure 10. Comparison among different algorithms for flux calculation against wind speed (LM86 corresponds to Liss and Merlivat (1986); other labels see in Table 4). Black dashed lines in min, mean and max denote the minimum, average and maximum monthly average wind speeds obtained from PenGaYi station in the ECS during the study period.

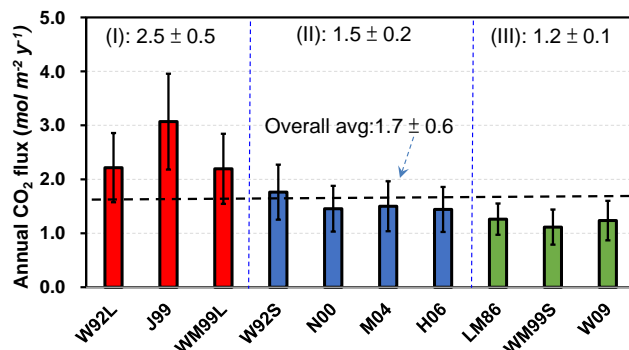


Figure 11. Comparison among the averaged annual CO_2 fluxes estimated by different algorithms in the study period. Three distinctive groups: (I) highest average: $-2.5 \pm 0.5 \text{ mol C m}^{-2} \text{ yr}^{-1}$; (II) mid-range: -1.5 ± 0.2 ; (III) low values: -1.2 ± 0.1 with an overall average: -1.7 ± 0.6 .

WM99L when the wind speed increases, while the algorithm developed by N00, M04 and H06 would not differ substantially, as compared to W92S (Fig. 10).

In Table 4, the summary of the averaged seasonal and annual CO_2 fluxes between 1998 and 2010 is shown for comparison, calculated from the above-mentioned 10 algorithms by using monthly wind speed data measured at PenGaYi station. Overall, the averaged annual CO_2 fluxes range between -1.1 ± 0.3 and $-3.1 \pm 0.9 \text{ mol C m}^{-2} \text{ yr}^{-1}$ with an average of -1.7 ± 0.6 . The flux results can be basically divided into three groups: (I) high values (avg: $-2.5 \pm 0.5 \text{ mol C m}^{-2} \text{ yr}^{-1}$) by J99, W92L, and WM99L; (II) mid-range values (-1.5 ± 0.2) by W92S, N00, M04 and

Table 4. Seasonal average CO₂ fluxes between 1998 and 2010 derived from the reported gas-transfer algorithms*.

Seasons	LM86*	W92L	W92S	WM99L	WM99S	J99	N00	M04
Spring	-3.0 ± 0.4	-4.6 ± 0.7	-3.7 ± 0.5	-4.5 ± 0.7	-2.3 ± 0.4	-6.4 ± 0.9	-3.0 ± 0.4	-3.1 ± 0.4
Summer	-0.6 ± 0.6	-1.4 ± 1.7	-1.1 ± 1.3	-1.3 ± 1.7	-0.6 ± 0.8	-1.9 ± 2.3	-0.9 ± 1.1	-1.0 ± 1.2
Fall	-0.2 ± 0.4	-0.4 ± 1.1	-0.3 ± 0.8	-0.4 ± 1.2	-0.2 ± 0.6	-0.6 ± 1.5	-0.3 ± 0.7	-0.3 ± 0.7
Winter	-1.9 ± 0.5	-3.1 ± 0.8	-2.5 ± 0.7	-3.4 ± 1.1	-1.7 ± 0.5	-4.3 ± 1.2	-2.0 ± 0.5	-1.9 ± 0.5
Annual	-1.3 ± 0.3	-2.2 ± 0.6	-1.8 ± 0.5	-2.2 ± 0.6	-1.1 ± 0.3	-3.1 ± 0.9	-1.5 ± 0.4	-1.5 ± 0.5
Seasons	H06	W09	Range (average)					
Spring	-3.0 ± 0.4	-2.6 ± 0.4	-2.3 to -6.4(-3.6)					
Summer	-0.9 ± 1.1	-0.8 ± 1.0	-0.6 to -1.9(-1.0)					
Fall	-0.3 ± 0.7	-0.2 ± 0.6	-0.2 to -0.6(-0.3)					
Winter	-2.0 ± 0.6	-1.7 ± 0.5	-1.7 to -4.3(-2.4)					
Annual	-1.4 ± 0.4	-1.2 ± 0.4	-1.1 to -3.1(-1.7)					

* Abbreviations denote references with gas-transfer equations:

LM86: Liss and Merlivat (1986), $k_{600} = 2.85 \times u - 9.65(3.6 < u < 13.0)$

W92L: Wanninkhof (1992, long-term), $k_{660} = 0.39 \times u^2$

W92S: Wanninkhof (1992, short-term), $k_{660} = 0.31 \times u^2$

WM99L: Wanninkhof and McGillis (1999, long-term), $k_{660} = 0.0283 \times u^3$

WM99S: Wanninkhof and McGillis (1999, short-term), $k_{660} = 1.09 \times u - 0.333 \times u^2 + 0.078 \times u^3$

J99: Jacobs et al. (1999), $k_{660} = 0.54 \times u^2$

N00: Nightingale et al. (2000), $k_{600} = 0.333 \times u + 0.222 \times u^2$

M04: McGillis et al. (2004), $k_{660} = 0.014 \times u^3 + 8.2$

H06: Ho et al. (2006), $k_{600} = 0.266 \times u^2$

W09: Wanninkhof et al. (2009), $k_{660} = 3 + 0.1 \times u - 0.064 \times u^2 + 0.011 \times u^3$

H06; and (III) low values (-1.2 ± 0.1) by LM86, WM99S and W09 (Fig. 11; Table 4). The results by W92L and WM99L are higher ca. 100 % than those by low values obtained from LM86, WM99S and W09. Among moderate values, differences in flux, compared to W92S, were not much for the algorithms developed by N00, M04 and H06 (20 % lower). The W92S was further chosen for comparison since it was widely used among the reported algorithms.

The seasonal CO₂ air–sea exchange fluxes estimated by the reported algorithms are summarized in Table 4, which highlights the differences in seasonal variability in the CO₂ sink in the ECS shelf among them. Annual CO₂ fluxes from seasonal field cruises in the ECS were also calculated by the W92S (Fig. 7d; Table 3). This is the first field data set to show the complete seasonal CO₂ flux in this region. The average annual flux was calculated to be $-1.9 (\pm 1.6, \text{seasonal variability}) \text{ mol C m}^{-2} \text{ yr}^{-1}$ with the seasonal flux ca. -3.4 , -0.9 ± 1.4 ($n = 3$), -0.2 , and $-3.0 \text{ mol C m}^{-2} \text{ yr}^{-1}$ for spring, summer, fall, and winter, which were almost the same as those estimated by model as shown in Table 4.

4 Conclusions

In this study, we have established an empirical relationship for predicting surface water $p\text{CO}_2$ in a river-dominated marginal ECS. The empirical algorithm for calculating $p\text{CO}_{2w}$ as a function of SST and CRD successfully simu-

lated the annual cycles of $p\text{CO}_{2w}$, $\delta p\text{CO}_2$ and the CO₂ flux, which are in excellent agreement with observations. The relation was further applied to the ECS shelf areas ($25\text{--}33.5^\circ \text{ N}$, $122\text{--}129^\circ \text{ E}$) by using remotely sensed data of SST and the estimated area of CRD. Overall, the annually averaged CO₂ uptake in 1998–2011 by the ECS shelf was constrained to about $1.8 \pm 0.5 \text{ mol C m}^{-2} \text{ yr}^{-1}$, based on observational data and model results, which were more representative than those reported previously. This assessment of annual CO₂ uptake surpasses all previous estimates in terms of temporal and spatial coverage, and, therefore, is more reliable. Thus, the ECS was annually a net sink of atmospheric CO₂ with a distinct seasonal pattern associated with interannual variations. The flux seasonality shows a strong sink in spring (i.e., March–May) and a weak source in late summer–mid-fall. The weak sink status during warm periods in summer–fall is fairly sensitive to changes of $p\text{CO}_2$ and may be easy to shift from a sink to a source altered by shrinkage of the plume area due to the CRD decreases through environmental changes under climate change and anthropogenic forcing. The impact of Changjiang runoff change on the ECS shelf CO₂ uptake capacity shall be, therefore, highlighted in near future.

The Supplement related to this article is available online at doi:10.5194/bg-11-3855-2014-supplement.

Acknowledgements. We thank the captains and crews of R/V *OR-I* for their assistance during LORECS cruises and G. C. Gong, project PI, for cruise logistic and hydrographic data support. Y.-F. Yeung, Y.-L. Chen, C.-S. Ji and Z.-Y. Luo assisted in lab work. This work was supported by the National Science Council (NSC, Taiwan) through grants, NSC 100 (101)-2611-M-002-004 (–015) and from the College of Science, National Taiwan University under the “Drunken Moon Lake Scientific Integrated Scientific Research Platform” grant, NTU#102R3252.

Edited by: F. Chai

References

- Cai, W. J., Dai, M. H., and Wang, Y. C.: Air-sea exchange of carbon dioxide in ocean margins: A province-based synthesis, *Geophys. Res. Lett.*, 33, L12603, doi:10.1029/2006GL026219, 2006.
- Chen, C. T. A. and Borges, A. V.: Reconciling opposing views on carbon cycling in the coastal ocean: Continental shelves as sinks and near-shore ecosystems as sources of atmospheric CO₂, *Deep-Sea Res. Pt. II*, 56, 578–590, 2009.
- Chou, W. C., Gong, G. C., Sheu, D. D., Hung, C. C., and Tseng, T. F.: Surface distributions of carbon chemistry parameters in the East China Sea in summer 2007, *J. Geophys. Res.*, 114, C07026, doi:10.1029/2008JC005128, 2009.
- Chou, W. C., Gong, G. C., Tseng, C. M., Sheu, D. D., Hung, C. C., Chang, L. P., and Wang, L. W.: The carbonate system in the East China Sea in winter, *Mar. Chem.*, 123, 44–55, 2011.
- Gong, G. C., Lee Chen, Y. L., and Liu, K. K.: Chemical hydrography and chlorophyll a distribution in the East China Sea in summer: implications in nutrient dynamics, *Cont. Shelf Res.*, 16, 1561–1590, 1996.
- Ho, D. T., Law, C. S., Smith, M. J., Schlosser, P., Harvey, M., and Hill, P.: Measurements of air-sea gas exchange at high wind speeds in the Southern Ocean: implications for global parameterizations, *Geophys. Res. Lett.*, 33, L16611, doi:10.1029/2006GL026817, 2006.
- Jacobs, C. M. J., Kohsiek, W., and Oost, W. A.: Air–sea fluxes and transfer velocity of CO₂ over the North Sea: results from ASGA-MAGE, *Tellus B*, 51, 629–641, 1999.
- Laruelle, G. G., Dürr, H. H., Slomp, C. P., and Borges, A. V.: Evaluation of sinks and sources of CO₂ in the global coastal ocean using a spatially-explicit typology of estuaries and continental shelves, *Geophys. Res. Lett.*, 37, L15607, doi:10.1029/2010GL043691, 2010.
- Liu, K. K., Peng, T. H., and Shaw, P. T.: Circulation and biological processes in the East China Sea and the vicinity of Taiwan: an overview and a brief synthesis, *Deep-Sea Res. Pt. II*, 50, 1055–1064, 2003.
- Liu, K.-K., Gong, G.-C., Wu, C.-R., and Lee, H.-J.: 3.2. The Kuroshio and the East China Sea, in: *Carbon and Nutrient Fluxes in Continental Margins: A Global Synthesis*, edited by: Liu, K.-K., Atkinson, L., Quiñones, R., and Talaue-McManus, L., IGBP Book Series, Springer, Berlin, 124–146, 2010.
- Liss, P. S. and Merlivat, L.: Air-sea gas exchange rates: Introduction and synthesis, in: *The Role of Air-Sea Exchange in Geochemical Cycling*, edited by: Buat-Ménard, P., NATO ASI series, Kluwer Academic Publishers, Holland, 113–127, 1986.
- McGillis, W. R., Edson, J. B., Zappa, C. J., Ware, J. D., McKenna, S. P., Terray, E. A., Hare, J. E., Fairall, C. W., Drennan, W., Donelan, M., DeGrandpre, M. D., Wanninkhof, R., and Feely, R. A.: Air-sea CO₂ exchange in the equatorial Pacific, *J. Geophys. Res.*, 109, C08S02, doi:10.1029/2003JC002256, 2004.
- Nightingale, P. D., Malin, G., Law, C. S., Watson, A. J., Liss, P. S., Liddicoat, M. I., Boutin, J., and Upstill-Goddard, R. C.: In situ evaluation of air-sea gas exchange parameterizations using novel conservative and volatile tracers, *Global Biogeochem. Cy.*, 14, 373–387, 2000.
- Peng, T. H., Hung, J. J., Wanninkhof, R., and Millero, F. J.: Carbon budget in the East China Sea in spring, *Tellus B*, 51, 531–540, 1999.
- Shim, J., Kim, D., Kang, Y. C., Lee, J. H., Jang, S.-T., and Kim, C.-H.: Seasonal variations in pCO₂ and its controlling factors in surface seawater of the northern East China Sea, *Cont. Shelf Res.*, 27, 2623–2636, 2007.
- Takahashi, T., Olafsson, J., Goddard, J. G., Chipman, D. W., and Sutherland, S.: Seasonal variation of CO₂ and nutrients in the high-latitude surface oceans: a comparative study, *Global Biogeochem. Cy.*, 7, 843–878, 1993.
- Tseng, C. M., Wong, G. T. F., Lin, I. I., Wu, C. L., and Liu, K. K.: A unique pattern in phytoplankton biomass in low-latitude waters in the South China Sea, *Geophys. Res. Lett.*, 32, L08608, doi:10.1029/2004GL022111, 2005.
- Tseng, C. M., Wong, G. T. F., Chou, W. C., Lee, B. S., Sheu, D. D., and Liu, K. K.: Temporal Variations in the carbonate system in the upper layer at the SEATS station, *Deep-Sea Res. Pt. II*, 54, 1448–1468, 2007.
- Tseng, C. M., Liu, K. K., Wang, L. W., and Gong, G. C.: Anomalous hydrographic and biological conditions in the northern South China Sea during the 1997–1998 El Niño and comparisons with the equatorial Pacific. *Deep-Sea Res. Pt. I*, 56, 2129–2143, doi:10.1016/j.dsr.2009.09.004, 2009a.
- Tseng, C. M., Gong, G. C., Wang, L. W., Liu, K. K., and Yang, Y.: Anomalous biogeochemical conditions in the northern South China Sea during the El-Niño events between 1997 and 2003, *Geophys. Res. Lett.*, 36, L14611, doi:10.1029/2009GL038252, 2009b.
- Tseng, C. M., Liu, K. K., Gong, G. C., Shen, P. Y., and Cai, W. J.: CO₂ uptake in the East China Sea relying on Changjiang runoff is prone to change. *Geophys. Res. Lett.*, 38, L24609, doi:10.1029/2011GL049774, 2011.
- Tsunogai, S., Watanabe, S., Nakamura, J., Ono, T., and Sato, T.: A preliminary study of carbon system in the East China Sea, *J. Oceanogr.*, 53, 9–17, 1997.
- Tsunogai, S., Watanabe, S., and Sato, T.: Is there a continental shelf pump for the absorption of atmospheric CO₂?, *Tellus B*, 51, 701–712, 1999.
- Walsh, J. J.: Importance of continental margins in the marine biological cycling of carbon and nitrogen. *Nature*, 350, 53–55, 1991.
- Wang, S. L., Chen, C. T. A., Hong, G. H., and Chung, C. S.: Carbon dioxide and related parameters in the East China Sea, *Cont. Shelf Res.*, 20, 525–544, 2000.
- Wanninkhof, R.: Relationship between wind speed and gas exchange over the ocean. *J. Geophys. Res.*, 97, 7373–7382, 1992.
- Wanninkhof, R. and McGillis, W. R.: A cubic relationship between air-sea CO₂ exchange and wind speed, *Geophys. Res. Lett.*, 26, 1889–1892, 1999.

- Wanninkhof, R. and Thoning, K.: Measurement of fugacity of CO₂ in surface water using continuous and discrete sampling methods, *Mar. Chem.*, 44, 189–204, 1993.
- Wanninkhof, R., Asher, W. E., Ho, D. T., Sweeney, C., and McGillis, W. R.: Advances in quantifying air-sea gas exchange and environmental forcing, *Annu. Rev. Mar. Sci.*, 1, 213–244, doi:10.1146/annurev.marine.010908.163742, 2009.
- Weiss, R. F.: Carbon dioxide in water and seawater: the solubility of a non-ideal gas, *Mar. Chem.*, 2, 203–215, 1974.
- Zhai, W. and Dai, M.: On the seasonal variation of air-sea CO₂ fluxes in the outer Changjiang (Yangtze River) Estuary, East China Sea, *Mar. Chem.*, 117, 2–10, 2009.